Occurrence climatology of equatorial plasma bubbles derived using FormoSat-3/COSMIC GPS radio occultation data

Ankur Kepkar[1,2], Christina Arras[2], Jens Wickert[1,2], Harald Schuh[1,2], Mahdi Alizadeh[1,3], and Lung-Chih Tsai[4]

[1]Technische Universität Berlin, Germany
[2]German Research Centre for Geosciences GFZ, Potsdam, Germany
[3]K.N. Toosi University of Technology, Tehran, Iran
[4]National Central University, Chung-Li, Taiwan

Correspondence: Ankur Kepkar (kepkar@gfz-potsdam.de)

Abstract. The GPS radio occultation technique (GPS-RO) is used to detect the equatorial plasma bubbles in the F-region of the ionosphere, which are characterized by depletion regions of plasma. Their occurrence climatology is derived using GPS-RO data from FormoSat-3/COSMIC between 2007 and 2017. The plasma bubbles are identified based on the S4 index derived from raw signal-to-noise ratio profiles. The analyses revealed that the F-region irregularities associated with the plasma bubbles occur mainly post-sunset close to the Earth's geomagnetic equator, and have peak shifting between America and Africa depending on different solar conditions. Besides, the plasma bubbles show a strong dependence on the solar cycle and have a significant distribution based on regions and seasons with maximum occurrence in Africa during March equinox during high solar activity. Similarly, from the vertical resolution provided by the radio occultation technique, we see a variation in the altitudinal extent with respect to the solar cycle. Through this paper, an attempt is made to show, that the GPS-RO can be used as a primary as well as a complementary technique for investigating this ionospheric phenomenon. Finally, the major advantage of using GPS-RO compared to other techniques is, that not only information on the plasma bubble occurrence but also its detailed altitude characteristics can be derived on a global scale.

1 Introduction

The Equatorial Plasma Bubbles (EPBs) are large regions of plasma depletion, which are prominent in the F-region of the ionosphere. These EPBs generally exist in clusters (Singh et al., 1997) and often deter the radio waves (e.g., GPS signals) penetrating through it, causing serious implication on its applications. These plasma bubbles primarily occur at low latitudes and induce rapid fluctuation in the amplitude as well as phase of the radio signals. This distortion of the signals is often termed as scintillation (Yeh and Liu, 1982). The EPBs instigated by plasma irregularities are also known by its generic name as Equatorial Spread F (ESF), which are perceived as a spread or diffused echoes in the ionosonde readings (Booker and

Wells, 1938; Whalen, 1997). Apart from scintillations in the radio signal, this irregularity manifests themselves as plume-like structures in the range time-intensity images from incoherent scatter radar (Kudeki and Bhattacharyya, 1999) and intensity bite-outs in airglow measurements (Sahai et al., 2000).

The EPBs are a night-time phenomenon and are initiated by means of the Rayleigh-Taylor Instability (RTI) mechanism in the bottomside of the F-layer (Sultan, 1996; Woodman, 2009). To trigger the RTI mechanism, various theories related to seed perturbation like atmospheric gravity waves (AGWs) as well as vertical shear of zonal plasma drift are considered amongst the likely source (Kudeki et al., 2007; Abdu et al., 2009; Huang et al., 2011; Taori et al., 2011). Other than these seed sources, off-equatorial ionospheric phenomena such as sporadic-E layers and medium scale traveling ionospheric disturbances have also been contemplated for possible seed activity along the equipotential magnetic field lines (Abdu et al., 2003; Tsunoda, 2007). However, the AGWs with wavelengths greater than 100 km are considered to have a significant impact in triggering the RTI by producing polarization electric field in the E-region, which then translates it onto the F-region along the magnetic field lines (Röttger, 1981; Tsunoda, 2010; Huang et al., 2011; Retterer and Roddy, 2014; Tsunoda, 2015). In the meanwhile, an important activity at the equator, i.e., Pre-Reversal Enhancement (PRE), plays a significant role in influencing the plasma bubble growth and vertically lifting it after the sunset. PRE is a phenomenon that causes an enhancement in the zonal eastward electric field at the sunset terminator before the electric field reverses in the westward direction during the night (Abadi et al., 2015). This enhancement in the eastward electric field creates a vertical electromagnetic (E x B) drift that influences the growth rate of RTI by lifting the plasma to heights where the ion-neutral collision rate is small (Farley et al., 1970; Fejer and Kelley, 1980; Abadi et al., 2015). The EPBs are known to occur within hours right after sunset, and the degree to which it extends in the latitude and altitude depends on the magnitude of PRE (Farley et al., 1970; Abdu et al., 2003; Abadi et al., 2015).

The depletions in the equatorial plasma were initially identified from in-situ measurements by Hanson and Sanatani (1973) and later confirmed by McClure et al. (1977). Ever since then, various techniques such as ground based observations (Woodman and La Hoz, 1976; Farley et al., 1970; Whalen, 1997; Kudeki and Bhattacharyya, 1999), airglow imagers (Sahai et al., 1994, 2000; Martinis and Mendillo, 2007), satellite-based in-situ measurements (Burke et al., 2004a; Park et al., 2005; Gentile et al., 2006; Stolle et al., 2006; Xiong et al., 2010; Dao et al., 2011) as well as Global Navigation Satellite Systems (GNSS) ground-based measurements (Basu et al., 1999; Carrano and Groves, 2007; Nishioka et al., 2008) have been used to study the EPBs. Although these techniques contributed enormously towards the understanding of the ionospheric irregularities, they lacked in providing critical information in one aspect or the other. For example, the ground-based sounders and GNSS ground receivers; although they provide crucial information related to the ionosphere and are globally distributed, they remain restricted to a landmass. On the other hand, the satellite-based in-situ instruments explore the prevailing conditions in the ionosphere along its orbital track but fail to provide crucial insight into the vertical ionospheric conditions. In recent times, the GPS-RO technique has been widely used for ionospheric investigation (Wickert et al., 2001; Arras et al., 2008; Wickert et al., 2009; Carter et al., 2013; Liu et al., 2016; Tsai et al., 2017). This is because of its extensive sounding capabilities along with high resolution measurements; both globally as well as vertically for envisaging four-dimensional prospect of the ionosphere.

The GPS-RO is a space-based technique, which involves two satellites, i.e., GPS and Low Earth Orbiting (LEO), operating on a high-low satellite satellite tracking (HL-SST) mode (Wickert et al., 2001, 2009). Its operational principle is mainly based

on LEO satellites tracking the radio signals from the GPS satellites, as they penetrate through the Earth's ionosphere and atmosphere, causing the signal to bend while crossing it. The fundamental observable, i.e., bending angle, obtained from bending of the signal at the point of closest approach to the Earth is measured as an additional Doppler shift for accurate frequency and orbit geometry measurements (Kursinski et al., 1997, 1999). In the ionosphere, the electron density profiles are obtained using the onion peeling algorithm (Lei et al., 2007). While, in the stratosphere and troposphere, temperature and pressure profiles are obtained through refractivity profiles (Wickert et al., 2002; Jakowski et al., 2004). In addition to providing such a wealth of information, this technique mitigates various technical shortcomings by operating under all weather conditions and providing long term stability without requiring calibration from time-to-time (Rocken et al., 1997). Due to GPS-LEO geometry, the GPS-RO technique provides measurements with a high vertical resolution that are globally distributed. In the past, various LEO missions contributed enormously towards radio occultation operations that led to the rise of one mission to another, starting from GPS/MET (GPS/METeorology), CHAMP (CHAllenging Minisatellite Payload), GRACE (GRAvity recovery and Climate Experiment), FormoSat-3/COSMIC (Formosa Satellite -3/Constellation Observing System for Meteorology, Ionosphere, and Climate) (Anthes et al., 2008; Wickert et al., 2009; Arras et al., 2010) to FormoSat-7/COSMIC 2 mission.

2 Data analysis

In this study, we use the measurements provided by FormoSat-3/COSMIC that perform global limb soundings using GPS-RO technique. The FormoSat-3/COSMIC mission is a constellation of six microsatellites, which provide $\sim 2,000$ continuous real-time neutral atmospheric and ionospheric profiles daily (Anthes et al., 2008). However, after orbiting for more than 13 years and exceeding its planned lifespan of five years, the number of RO profiles has significantly reduced to approximately 20% since the middle of 2016. This is because currently only one out of six satellites is operational under degraded mode (Chu et al., 2018). Nevertheless, this study comprises of measurements taken during the years 2007-2017 that includes nearly 5.5 million ionospheric profiles.

For our investigations, we use *ionPhs* (*ion*ospheric excess *Phas*es) data which belong to *level 1b* dataset. These FormoSat-3/COSMIC observation files are freely available on the web portal of COSMIC Data Analysis and Archival Center (CDAAC) database, which are managed by University Corporation for Atmospheric Research (UCAR), Colorado, United States of America. In addition, CDAAC also provides *'ScnLv1'* scintillation datasets, which contains off-line constructed S4 data calculated from $50\,\mathrm{Hz}$ that are recorded at $1\,\mathrm{Hz}$. But from the several thousand *ScnLv1* profiles that are retrieved daily, only less than one-fourth profiles can be reconstructed for the F-region altitude of the ionosphere (Tsai et al., 2017). Thus exploiting *ionPhs* dataset is justifiable, which are almost five times more than the *ScnLv1*. The derivation of *ionPhs* profiles is based on the assumption of spherical symmetry; however, it is not valid for EPBs (Jakowski et al., 2004; Arras, 2010). These *ionPhs* datasets are retrieved at $1\,\mathrm{Hz}$ sampling rate with $\sim 2\,\mathrm{km}$ of altitude resolution along the vertical range of $\sim 60\,\mathrm{km}$ above Earth's surface up to the orbital height of the LEO ($\sim 800\,\mathrm{km}$).

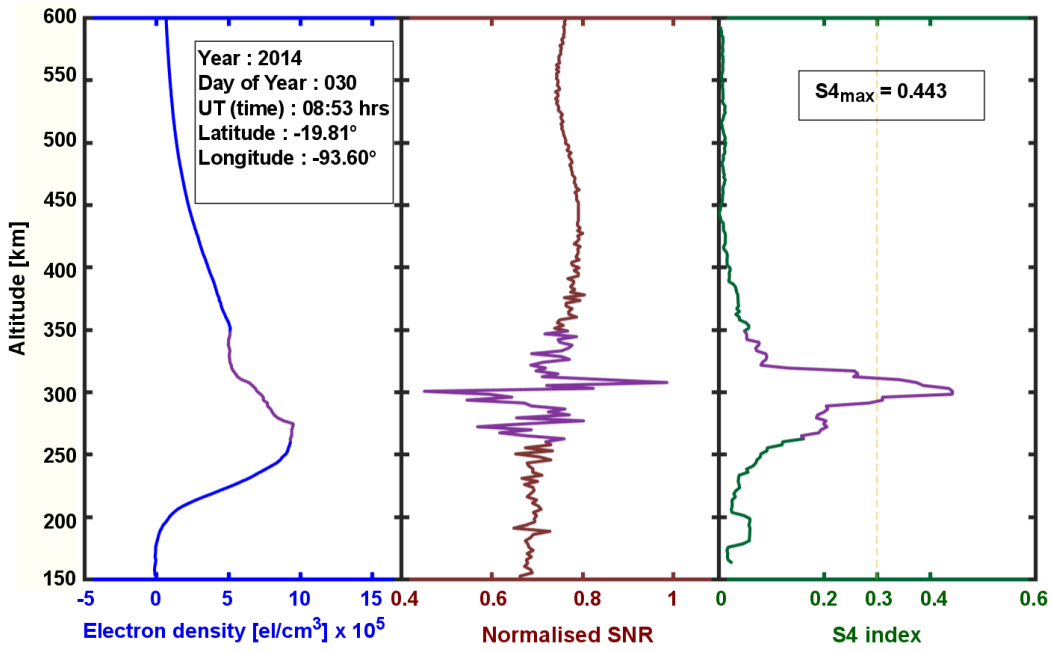

Figure 1. Electron density profile (ionPrf product) in conjunction with normalized SNR and derived S4 index (ionPhs product). The purple color line in the plot shows depletion in electron density and corresponding fluctuations of normalized SNR profile and high index values in the S4 plot.

In particular, we make use of the raw Signal-to-Noise ratio (SNR) of the GPS L1 ($1,575\,\mathrm{MHz}$) *ionPhs* measurements. This is because the L1 measurements show strong signal characteristics, and are received with a relatively higher intensity when compared to the GPS L2 ($1,227\,\mathrm{MHz}$) signals which are weaker and noisier. On the other aspect, SNR measurements are preferred over electron density profiles since they are straightway available and no further treatment is required. Additionally, from literature we know, that amplitude variation in the SNR profile has a direct influence on the vertical gradient of the electron density which provides critical information on the underlying space weather conditions (Wickert et al., 2004; Arras et al., 2008). From Fig. 1 it is visible that the EPB's signature characterized by sharp depletion in the electron density corresponds to strong oscillations in the SNR profiles. Subsequently, a high amplitude scintillation index is derived from these fluctuations.

The scintillations caused by plasma bubbles are identified by deriving amplitude scintillation index, i.e., S4 index, from the SNR of the GPS L1 signals. This is because the variations in the SNR can be associated with the vertical changes in the electron density that mainly occur in line with the irregularities, for example, the EPBs (Hajj et al., 2002; Arras and Wickert, 2018). For subsequent analyses of the plasma bubble, attributes such as SNR of GPS L1 signal, Universal time, altitude, latitude, and

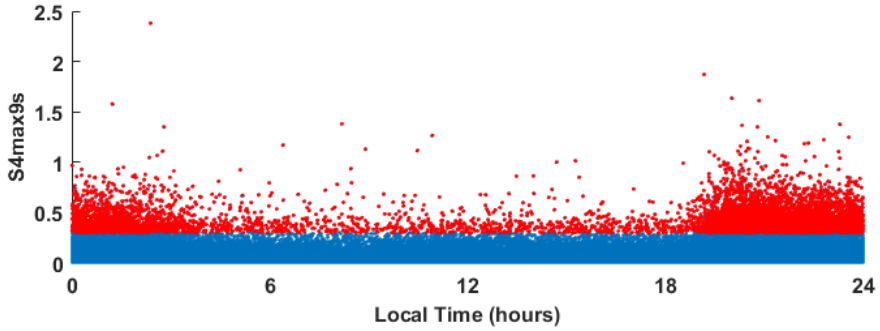

Figure 2. Plot of $S4max9sec$ as a function of local time (LT) during 2014. The blue dots represent the scintillation index less than 0.3, whereas strong scintillations are represented by the red dots having S4 index larger than 0.3.

longitude are extracted from the *ionPhs* datasets. Following that, the S4 index is computed from the raw SNR measurements as described by Syndergaard (2006) in Eq. 1.

$$S4max9sec = \frac{\sqrt{\left\langle \left(I - \left\langle \bar{I} \right\rangle \right)^2 \right\rangle}}{\left\langle \bar{I} \right\rangle} \tag{1}$$

where $S4max9sec$ denotes the scintillation index calculated over nine seconds interval, *I* is the square of the Signal-to-Noise (SNR) ratio of L1 GPS signal, and the bracket $\langle\rangle$ stands for average taken over nine seconds. In addition, a low pass filter is applied to the time series of nine seconds interval to obtain a new average of the intensity $\langle \bar{I} \rangle$ for constructing a long-term detrended $S4max9sec$ index (Syndergaard, 2006).

A simple representation of $S4max9sec$ versus local time during the year 2014 is depicted in Fig. 2, which shows scattered scintillation values caused due to varying electron density gradient. Additionally, it also highlights low $S4max9sec$ values during the day and high values during the night. The high values, usually observed during the night, are due to the plasma instabilities in the F-region after sunset. Altogether about 0.5 million profiles were retrieved in 2014, out of which only 6,130 (i.e., $\sim 1.2\%$) global profiles were classified as strong scintillation events originating from possible plasma instabilities.

For this study, we classified scintillation events based on different $S4max9sec$ index. Hereafter $S4max9sec$ index will be referred to as the S4 index and the same is presented in Table 1 along with different scintillation categories. Within this study, we consider the S4 index greater than 0.3 to quantify strong scintillation events influenced by possible plasma bubbles (Brahmanandam et al., 2012; Carter et al., 2013).

***S4* values**	**scintillation category**	**occurrence (2014)**
$S4 \geq 1.0$	high	0.02%
$0.3 < S4 < 1$	moderate	1.19 %
$S4 \leq 0.3$	low	98.79%

Table 1. Categorization of S4 index intensity.

3 Results

The FormoSat-3/COSMIC measurements between mid-2007 and 2017 are exploited to understand the occurrence of EPBs. In this study, we used COSMIC measurements starting from June 2007. This time-interval was selected to avoid the influence of orbit maneuvers in the data which were present until May 2007. Since the FormoSat-3/COSMIC satellites fly in non-sun-synchronous orbit, they effectively perform global soundings. However, in order to centralize this study in the equatorial region, we only consider the measurements within the latitudinal extent of 50° N/S. By determining this limit, we exclude the polar scintillation events and lay focus on the equatorial ones. Also, we set the altitude range between $150\,$km and $600\,$km to avoid the influence from the E-region and the noisier information from the GPS-RO profiles above $600\,$km.

3.1 Global distribution of EPBs

The EPBs are field align irregularities, which occur along the geomagnetic equator and peaks during the time of year when the magnetic field lines are closely aligned with the sunset terminator (Tsunoda, 1980, 1985). A global occurrence climatology of the EPBs for almost 11 years is presented in Fig. 3. It shows that the EPBs follow the course of the magnetic equator along with longitude dependence for different years, comparable to the morphology of F-region scintillations presented by Tsai et al. (2017). The EPB occurrence rate is calculated as a ratio of a number of profiles having S4 index greater than 0.3 to a number of all RO profiles within the specified grid integrated over the complete local time range. Furthermore, the 11-year climatology corresponds to the solar cycle outlining the descending-ascending-descending phase. As we proceed towards the solar minimum year 2009, i.e., descending phase, we see the EPB occurrence rate declining with the peak appearing in the South American sector. Whereas, as we advance towards the solar maximum year 2014, i.e., ascending phase, the EPB occurrence rate increases gradually with the peak stretching along the Atlantic-African region with each passing year. However, as we approach towards the next descending phase, it is again noticeable, that the EPB occurrence rate decreases with the peak migrating towards the South American region. Throughout this climatology, we see that a finite proportion, if not the peak occurrence, of EPBs are present in the South American region. One of the reasons conferred by Huang et al. (2001) suggests the existence of a weaker magnetic field in that region, which accounts for RTI irregularities caused due to vertical plasma drift because of the zonal electric field during the sunset. On the contrary, Burke et al. (2004a) argued on the weak occurrence rates of EPB during high solar activity citing reason towards increased E-region conductivity because of particle precipitation in the South Atlantic anomaly. Besides, McClure et al. (1998) proposed possible seeding from the gravity waves emerging from the troposphere in the Andes, which has been investigated by Su et al. (2014). The author confirmed a very good correlation only in the South American region due to gravity waves originating in the intertropical convergence zone. However, in the Atlantic-African region, there was a positive but still weak correlation. For such correlations, the author implied, that in addition to gravity waves, there could be other seed perturbations causing plasma instabilities. From the year-wise EPB occurrence, we

observe that towards low solar activity almost negligible EPB occurrence is observed in the Atlantic-African, Asian, and Pacific region. This signifies possible association of PRE to seed the EPBs in this region since we know that the magnitude of PRE is largely affected by solar activity (Stolle et al., 2008; Abadi et al., 2015). Thus we recognize the substantial occurrence of EPBs during high solar activity when the PRE has its peak magnitude, while a very weak occurrence rate of EPBs exists during low solar activity when the PRE amplitude is also at its minimum.

3.2 Local time dependency

From the previous studies based on various probing techniques, it is evident that the EPBs are a night-time phenomenon, that includes small scale irregularities inside the bubble that lead to turbulent structures causing scintillations (Woodman and La Hoz, 1976; Whalen, 1997; Sahai et al., 2000; Gentile et al., 2006; Yokoyama, 2017). A general local time occurrence of EPBs during 2014 is presented in Fig. 4. This local time representation of EPBs is based on the global soundings retrieved from the FormoSat-3/COSMIC satellites which fly in non-sun-synchronous orbit. The EPB occurrence rate is based on calculation similar to the global distribution occurrence, but for a different grid composition. It is clear from the Local Time (LT) representation, that the EPBs develop around 19:00 LT shortly after the sunset when the polarization electric field shorts E-region conductivity causing a rapid loss of plasma, which is similar to the results affirmed by Stolle et al. (2006) using CHAMP in-situ measurements. In general, we know that a substantial occurrence rate is observed during the high solar activity year, while fewer EPBs are generated during low solar activity year (Basu et al., 2002). In Fig. 5, we present a closer look at the occurrence of EPBs based on solar maximum (2014) and solar minimum (2009) year. The occurrence rate is calculated as a ratio of the S4 values greater than 0.3 to the total number of S4 profiles for a particular hour bin starting from 19:00 LT. From the analysis we can witness, that during solar maximum the EPBs culminate approximately one hour earlier, i.e., 21:00 LT, than what is observed during solar minimum year, i.e., 22:00 LT; which is in agreement with the EPBs detected using CHAMP and GRACE in-situ measurements by Xiong et al. (2010). However, our local time occurrence slightly differs from the local time distribution presented by Carter et al. (2013); wherein in his analysis, a high solar activity year peaks about an hour later than the solar minimum year for all season-longitude. The local time occurrence characteristics presented in this paper agree well with the argument conferred by Burke et al. (2009) who suggests, that the slow process of gravity-driven currents over weak PRE magnitude influences the EPB occurrence to peak at a relatively later local time for the solar minimum year.

3.2.1 Region-wise seasonal dependence of EPBs

Based on the argument put forth by Tsunoda (1985), we know that the region-wise seasonal occurrence of plasma bubbles depends on the close alignment of the magnetic field line with the sunset terminator. In order to analyze the region-wise seasonal occurrence characteristics of EPB, the longitude extent is discretized in four different sectors of 90° each, which includes America (110°W-20°W), Africa (20°W-70°E), Asia (70°E-160°E) and Pacific (160°E-110°W). These longitude sectors are further compared with different seasons based on three-month interval around each solstice and equinox. The region-wise seasonal occurrence is based on geomagnetic latitude with respect to local time and envisaged in Fig. 6 which is similar to the seasonal-longitude occurrence presented for solar minimum conditions (2007-2011) by Carter et al. (2013). In

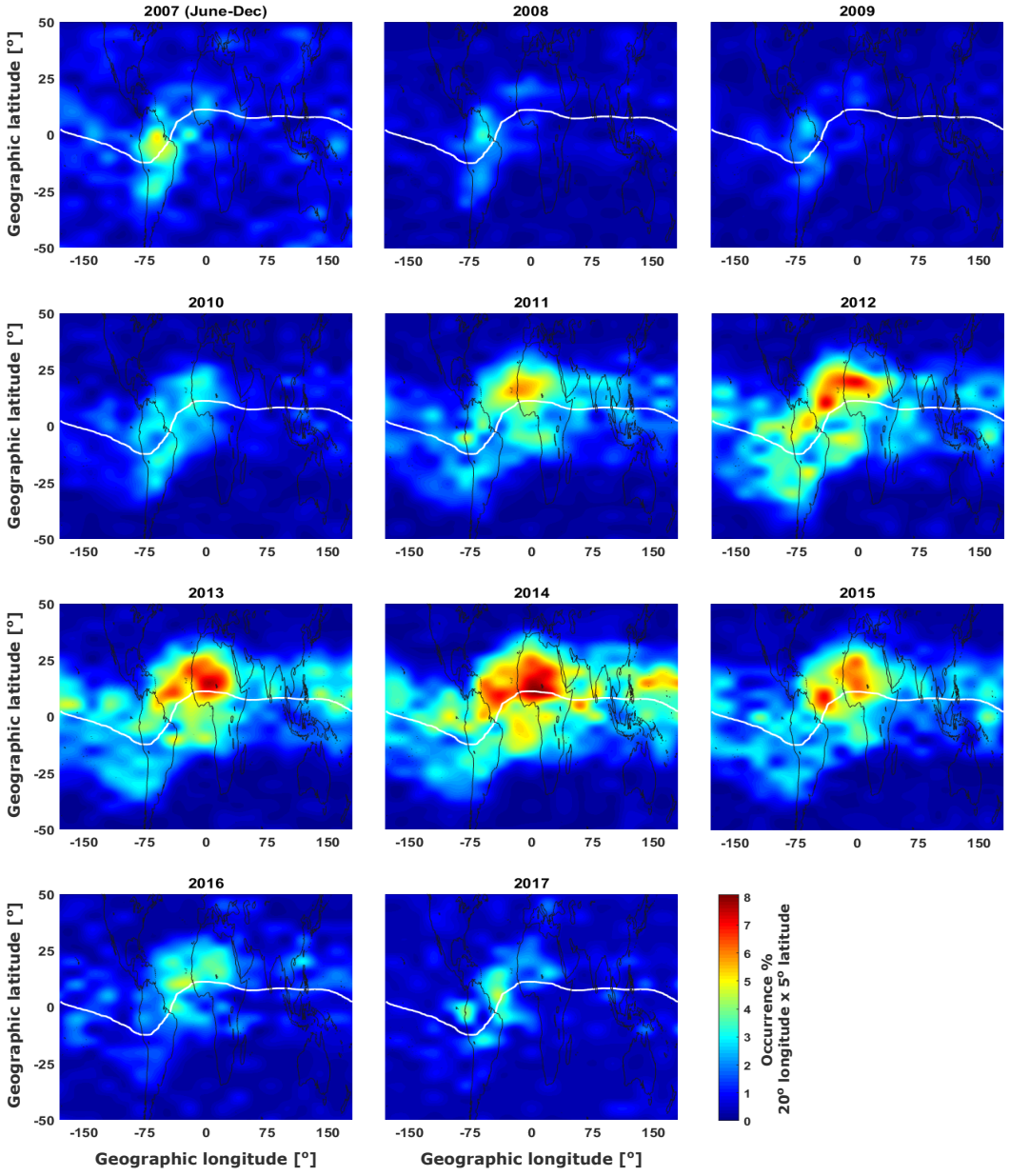

Figure 3. Plot of geographical latitude [°] v/s geographical longitude [°] of EPBs from mid-of 2007 to 2017. The white solid line depicts the geomagnetic equator.

comparison, in this study around 2.2 million profiles are analyzed to present EPB's distribution between 2012-2016 covering the crest of the solar cycle 24, i.e., 2014. In general, we observe that the EPBs are distributed on either side of the dip equator with only one maximum on the positive side of the dip equator across all longitudes and seasons. On the contrary, two maxima on either side of the dip equator were observed by Carter et al. (2013) during solar minimum condition using FormoSat-

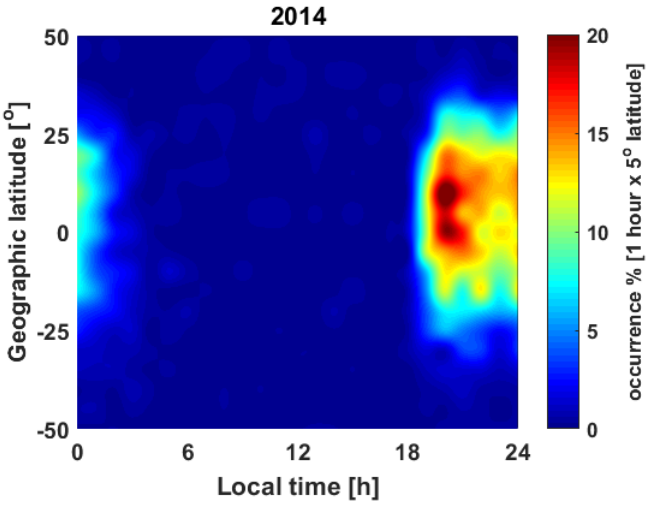

Figure 4. Local time dependence of equatorial plasma bubble occurrence during 2014.

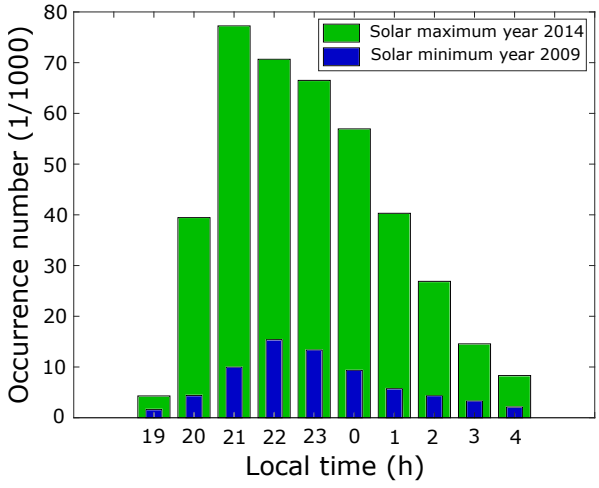

Figure 5. Occurrence of plasma bubbles based on local time during the solar minimum year (2009) and solar maximum year (2014) respectively.

3/COSMIC data, whereas only one peak at the dip equator was observed by Burke et al. (2004a) with Republic of China SATellite (ROCSAT)-1 observations in the period 2000-2002. In the American region, we see the substantial occurrence of EPBs across all the seasons, except the June solstice (May-June-July). Whereas in the African region, we see the comparable occurrence of EPBs across all the season but the least number of EPBs in the December solstice. Across all longitude sectors, the least occurrence of EPBs was recorded in Asia for most of the seasons. In principle, maximum occurrence during both equinoxes are observed in Africa and agrees well with the results presented by Burke et al. (2004b) and Su et al. (2008); but

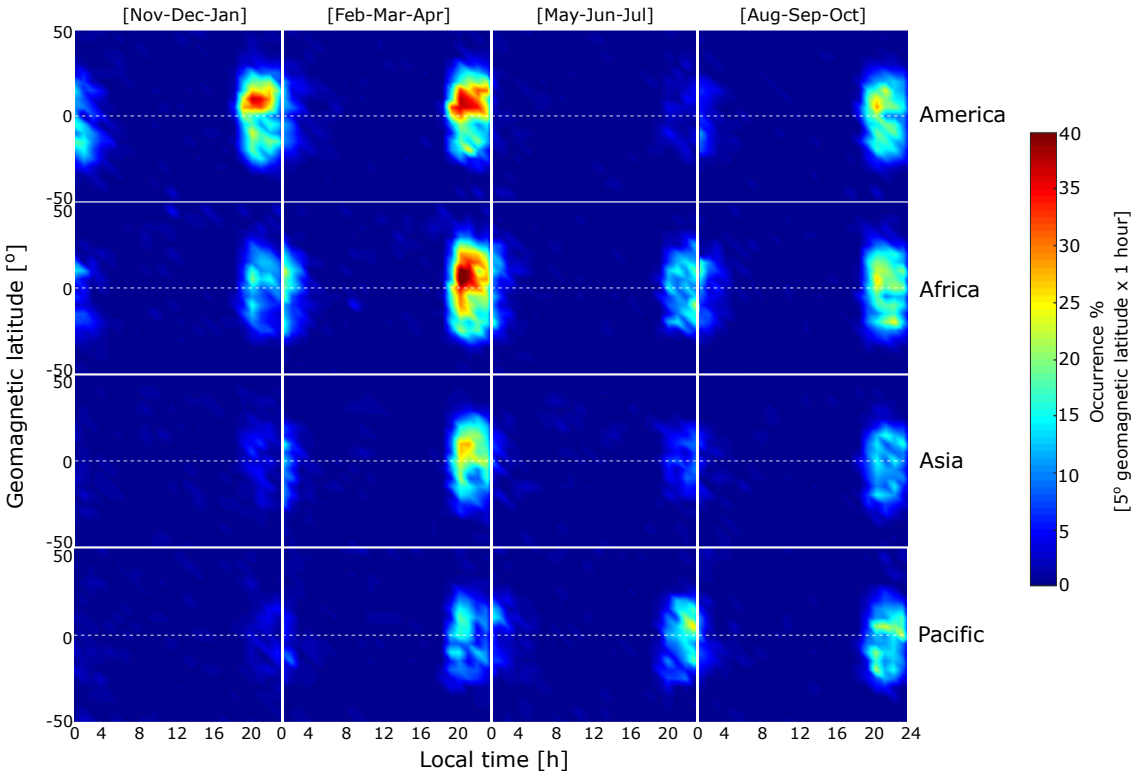

Figure 6. EPBs occurrence during the years 2012-2016 for different longitude sectors (regions) based on three-month intervals (season). White dashed lines represent geomagnetic dip equator.

it defers from the maximum equinoctial occurrence in America presented by Carter et al. (2013). This discrepancy for the maximum equinoctial occurrence could arise due to measurements involving different solar conditions; wherein during solar minimum conditions peak occurrence was observed in the American region (Carter et al., 2013), whereas during high solar activity we see peak occurrence in the African region.

Furthermore, we see asymmetries in the equinox and solstice seasons. For example, we observe negligible EPBs during June solstice in the American sector compared to the rest of the seasons. This is because of the larger sunset time lag in the former that abstains from the formation of EPBs according to the hypothesis presented by Tsunoda (1985). Whereas more EPBs are seen during the June solstice than the December solstice in Africa, Asia, and Pacific region. But for this scenario, the sunset time lag approach could not justify the occurrence; however it was rationalized by Nishioka et al. (2008) citing the reason towards the integrated flux tube conductivities in the F-region and its seasonal occurrence which proved to be favorable for the solstice asymmetry in Africa, Asia, and Pacific sectors. On the aspect of equinox asymmetry, we see significant occurrence in March equinox (February-March-April) than September equinox (August-September-October) in America, Africa, and Asia, except the Pacific region and agrees well with Burke et al. (2004b). In general, few EPBs are recorded in the region where the

strength of the equatorial magnetic field is strong in the Eastern hemisphere, e.g., Asian and parts of Pacific sectors. Whereas comparably more EPBs are observed in the region of a relatively weak equatorial magnetic field, i.e., American and African longitudes (Burke et al., 2004a, b).

3.3 Altitude variations and solar cycle dependency

The FormoSat-3/COSMIC measurements provide height dependent information, which is valuable as compared to the measurements from the other contemporary techniques for investigating plasma bubbles on a global scale. From the generalized notion, we know that the EPBs are generated in the bottomside of the F-region as a consequence of RTI and move upwards by means of the electrodynamic process (Whalen, 1997; Kelley, 2009; Woodman, 2009). For manifestation, we present the altitude distribution of EPBs in Fig. 7 on a year-wise basis. It is noticeable that the year-wise altitudinal distribution occurs in accordance with the different conditions of solar activity. The study also reveals that the periodic variation in the solar cycle plays an indirect role in influencing the vertical occurrence range of the plasma bubbles; wherein a large range is covered during high solar activity, i.e., 2014 and lesser altitude range during low solar activity, i.e., 2009. Besides, we observe peak occurrence at an altitude of $\sim 420\,$km during 2014, and $\sim 240\,$km during 2009. The extent to which the EPBs are uplifted in the altitude is motivated by the magnitude of the PRE which depends on the solar activity (Fejer et al., 1999; Stolle et al., 2008; Abadi et al., 2015; Liu et al., 2016). In addition, the EPBs which are primarily generated at the geomagnetic equator elongates in latitude due to the dominance of PRE (Abdu et al., 2003; Liu et al., 2016). This is obvious in the altitude distribution of the plasma bubbles; wherein during low solar activity the EPBs are almost contained at the geomagnetic equator, while during high solar activity the EPBs are spread out on either side of dip equator Liu et al. (2016). The seed perturbation along with the altitudinal variation of the EPBs is largely attributed to the PRE phenomenon which is an outcome of degenerated conductivity in the E-region along with enhanced zonal electric field at the sunset (Farley et al., 1970; Stolle et al., 2008; Su et al., 2014). Ideally, the PRE lifts the plasma in the F-layer by means of E$\times$B drift to an altitude where the neutral-ion collision frequency is low which is inversely proportional to the growth rate of plasma bubble (Fejer et al., 1999; Abadi et al., 2015). In the process, the EPBs continue to proceed higher in altitude until the eastward electric field on the top of the bubble becomes zero and eventually they decay (Krall et al., 2010).

From the occurrence climatology presented in this paper, it is apparent that the EPBs materialize in accordance with the solar activity by the influence of the seed perturbation such as PRE. Thus more EPBs are detected during maximum solar activity than the minimum (Basu et al., 2002). A brief analogy is presented in Fig. 8 in support with the argument, which shows the sunspot cycle and relative occurrence numbers of EPBs with semi-annual structures across different years. Further, Fig. 8a depicts the current sunspot cycle represented by the monthly number of sunspots (blue solid line) and a smoothed curve (orange solid line), whereas Fig. 8b shows an annual occurrence trend of plasma bubbles characterized by monthly (red solid line) and smoothed monthly values (green solid line) from mid-of 2007 to 2017. On the global spectrum, the EPBs occur in line with the solar activity; however, it is not a conventional scenario on a regional basis. Nishioka et al. (2008) showed that the influence of solar conditions is bounded to a particular region and season. For example, the EPBs in the African and Asian sectors appear in congruence with the solar cycle; however the same is not observed in the American sector as revealed in Fig.

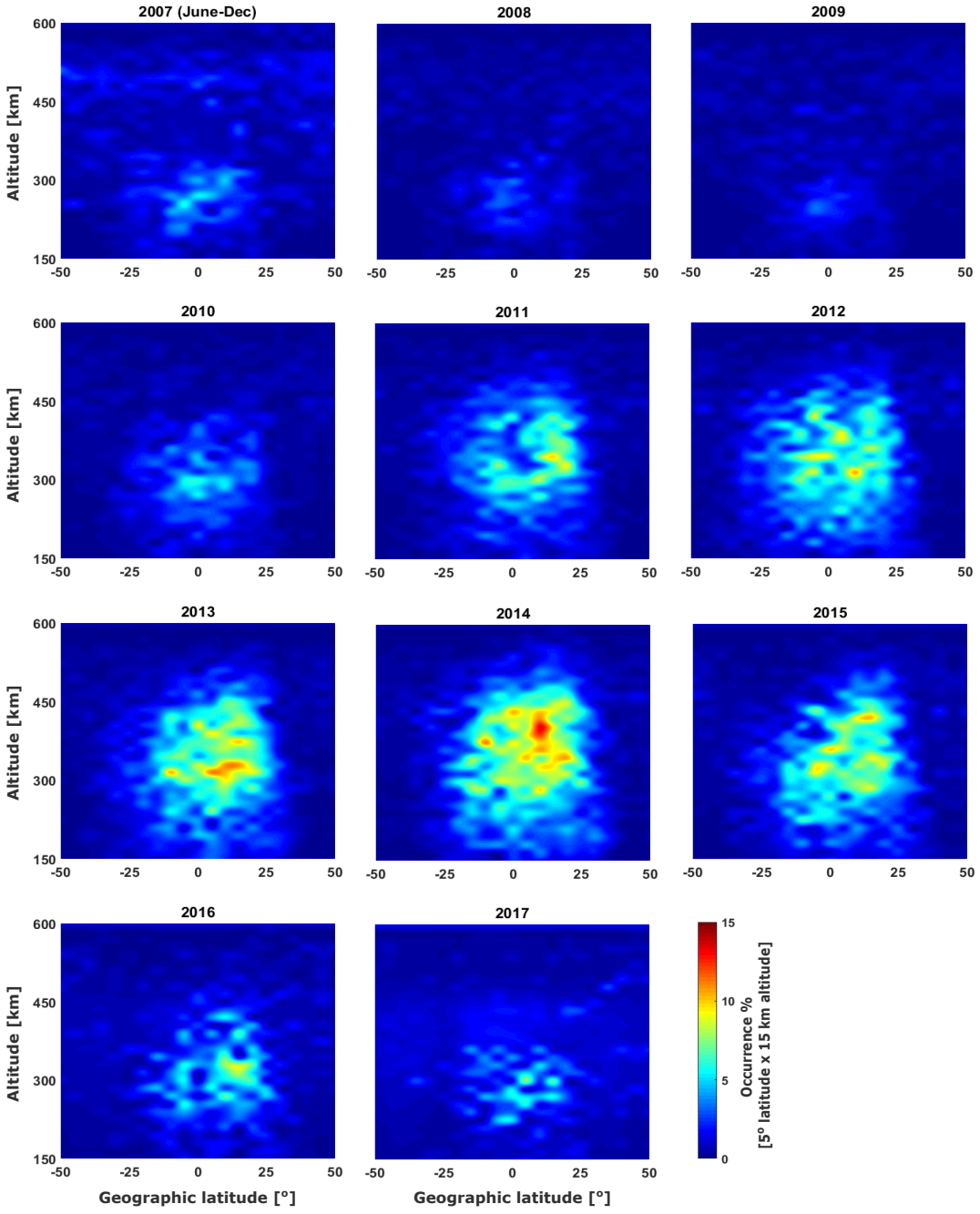

Figure 7. Plot of geographical latitude v/s altitude of equatorial plasma bubbles for showing vertical distribution during the years between mid-of 2007 and 2017.

3. This could most likely be due to the presence of gravity wave perturbations, which seed EPBs despite weak PRE magnitudes during solar minimum conditions in the South American region (Burke et al., 2004a; Stolle et al., 2008; Su et al., 2014).

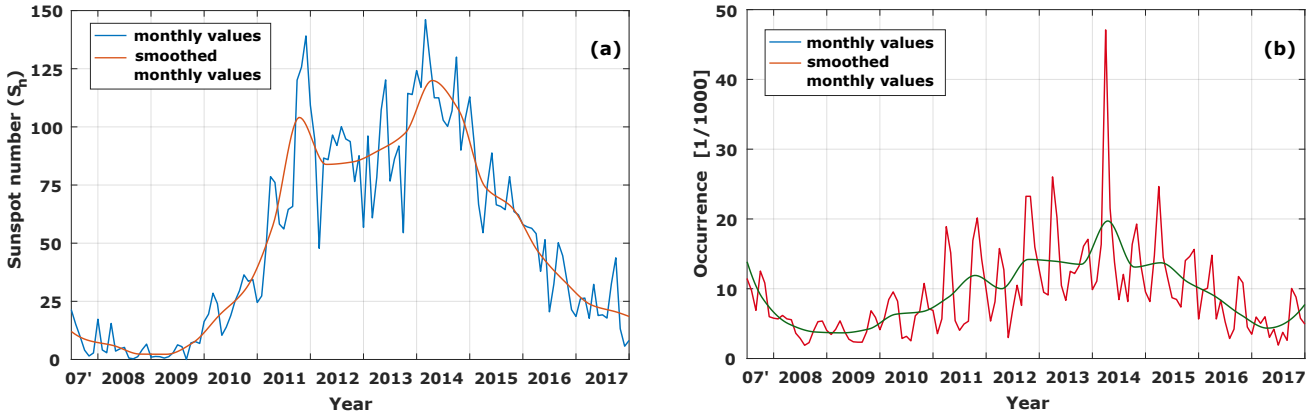

Figure 8. Comparison plot of (a) Sunspot cycle (b) Occurrence trend of equatorial plasma bubbles from mid-of 2007 to 2017, having monthly values and smoothed monthly values using low pass filter.

4 Conclusions

This paper provides a brief occurrence climatology of EPBs covering around 10.5 years of GPS-RO measurements derived from FormoSat-3/COSMIC. The scintillations induced in the radio waves caused by the EPBs are detected using amplitude scintillation index known as the S4 index. By classifying the S4 data, subsequent analyses are carried out by exploiting the strong scintillation events. In this study, we see that the EPBs occurring along the geomagnetic equator have peak occurrence oscillating between America and Africa during solar minimum and solar maximum years respectively. Furthermore, the year-wise global distribution of EPBs shows good congruency with solar activity, especially in Africa. Thus implying on the influence of vertical drift from PRE which also depends on the solar activity. However, there is no clear dependency of the solar cycle in the American sector. On hindsight, it is also known, that gravity-driven current has a strong correlation on the occurrence of a plasma bubble only in the American sector. Therefore, it is presupposed that the EPBs are triggered with different seed perturbations for different regions. Apart from the global distribution of EPBs, we know that the EPBs develop post-sunset around 19:00 LT, right after the enhancement in the zonal eastward electric field at the sunset. From the local time of the EPB occurrence for different solar conditions, it is observed that the EPBs generated during solar maximum year peaks earlier than the EPBs during the solar minimum year. This implicates the dependency on PRE which has a stronger magnitude of vertical plasma drift during high solar activity than during low solar activity. On the other hand, when we analyzed region-wise seasonal occurrence, we observed maximum EPBs in Africa during March equinox. Almost in all longitude sectors, more EPBs were detected in the March equinox than the September equinox. Whereas for solstice months it justifies the argument from Tsunoda (1985), wherein more EPBs are encountered at longitudes with positive (negative) declination during June (December) solstice and have good agreement with Burke et al. (2004b), Su et al. (2008), and Carter et al. (2013). Recently it was articulated by Xiong et al. (2010) through his comparative study of EPBs using CHAMP and GRACE in-situ measurements, that more EPBs are encountered at an altitude below 300 km than above. However, since the in-situ measurements detect the EPBs at its

orbital altitude which is usually above $\sim 400\,\mathrm{km}$, some signatures of EPBs are merely detected. Thus, the GPS-RO becomes convenient for investigating the EPBs for their vertical soundings at the same time providing global resolution. Meanwhile, these EPBs which are provoked by PRE show a strong dependence on the periodic variation in the solar activity with a larger altitude extent as we proceed towards the high solar activity. In principle, we observe that, throughout the global analyses, the annual EPBs occurrence have a strong dependency on solar activity, which was additionally compared with the sunspot cycle. Overall, the GPS-RO technique seems favorable in understanding the EPBs and could be used as a complementary technique in analyzing such ionospheric irregularities because of its unique measurements as a result of vertical scans.

Code availability. TEXT

Data availability. Ionospheric radio occultation data is based on FormoSat-3/COSMIC satellite mission available from CDAAC (http://www.cosmic.ucar.edu). The dataset for the solar sunspot number is obtained from Sunspot Index and Long term Solar Observations website (http://www.sidc.be/silso/datafiles)

Appendix A

A1

Author contributions. A. Kepkar performed the analysis and drafted the manuscript with the help of C. Arras and J. Wickert. H. Schuh, M. Alizadeh and L.C. Tsai provided with constructive scientific advices.

Competing interests. The authors declare that they have no conflict of interest.

Disclaimer. TEXT

Acknowledgements. The authors recognize the efforts of FormoSat-3/COSMIC team and are grateful for providing the measurements. C. Arras acknowledges the support from Deutsche Forschungsgemeinschaft (DFG) Priority Program DynamicEarth SPP1788. A. Kepkar acknowledges support from DFG under SCHU 1103/15-1.

References

Abadi, P., Otsuka, Y., and Tsugawa, T.: Effects of pre-reversal enhancement of E×B drift on the latitudinal extension of plasma bubble in Southeast Asia, Earth, Planets and Space, 67, 74, https://doi.org/10.1186/s40623-015-0246-7, 2015.

Abdu, M., MacDougall, J., Batista, I., Sobral, J., and Jayachandran, P.: Equatorial evening prereversal electric field enhancement and sporadic E layer disruption: A manifestation of E and F region coupling, Journal of Geophysical Research: Space Physics, 108, 1254–1267, https://doi.org/10.1029/2002JA009285, 2003.

Abdu, M., Kherani, E. A., Batista, I., de Paula, E., Fritts, D., and Sobral, J.: Gravity wave initiation of equatorial spread F/plasma bubble irregularities based on observational data from the SpreadFEx campaign, Annales Geophysicae, 27, 2607–2622, https://doi.org/10.5194/angeo-27-2607-2009, 2009.

Anthes, R. A., Bernhardt, P. A., Chen, Y., Cucurull, L., Dymond, K. F., Ector, D., Healy, S. B., Ho, S. P., Hunt, D. C., Kuo, Y. H., Liu, H., Ko, M., McCormick, C., Meehan, T., Randel, W. J., Rocken, C., Schreiner, W. S., Sokolovskiy, S. V., Syndergaard, S., Thompson, D. C., Trenberth, K. E., Wee, T. K., Yen, N. L., and Zeng, Z.: The COSMIC/FORMOSAT-3 mission: Early results, Bulletin of the American Meteorological Society, 89, 313–333, https://doi.org/10.1175/BAMS-89-3-313, 2008.

Arras, C.: A Global Survey of Sporadic E Layers based on GPS Radio Occultations by CHAMP, GRACE and FORMOSAT-3/COSMIC, Scientific Technical Report (STR) 10/09, German Research Centre for Geosciences (GFZ), Potsdam, https://doi.org/10.2312/GFZ.b103-10097, 2010.

Arras, C. and Wickert, J.: Estimation of ionospheric sporadic E intensities from GPS radio occultation measurements, Journal of Atmospheric and Solar-Terrestrial Physics, 171, 60–63, https://doi.org/10.1016/j.jastp.2017.08.006., 2018.

Arras, C., Wickert, J., Beyerle, G., Heise, S., Schmidt, T., and Jacobi, C.: A global climatology of ionospheric irregularities derived from GPS radio occultation, Geophysical Research Letters, 35, L14 809, https://doi.org/10.1029/2008GL034158, 2008.

Arras, C., Jacobi, C., Wickert, J., Heise, S., and Schmidt, T.: Sporadic E signatures revealed from multi-satellite radio occultation measurements, Advances in Radio Science, 8, 225–230, https://doi.org/10.5194/ars-8-225-2010, 2010.

Basu, S., Groves, K., Quinn, J., and Doherty, P.: A comparison of TEC fluctuations and scintillations at Ascension Island, Journal of Atmospheric and Solar-Terrestrial Physics, 61, 1219–1226, https://doi.org/10.1016/S1364-6826(99)00052-8, 1999.

Basu, S., Groves, K., Basu, S., and Sultan, P.: Specification and forecasting of scintillations in communication/navigation links: current status and future plans, Journal of atmospheric and solar-terrestrial physics, 64, 1745–1754, https://doi.org/10.1016/S1364-6826(02)00124-4, 2002.

Booker, H. and Wells, H.: Scattering of radio waves by the F-region of the ionosphere, Journal of Geophysical Research, 43, 249–256, https://doi.org/10.1029/TE043i00-3p00249, 1938.

Brahmanandam, P., Uma, G., Liu, J., Chu, Y., Latha Devi, N., and Kakinami, Y.: Global S4 index variations observed using FORMOSAT-3/COSMIC GPS RO technique during a solar minimum year, Journal of Geophysical Research: Space Physics, 117, A09 322, https://doi.org/10.1029/2012JA017966, 2012.

Burke, W., Gentile, L., Huang, C., Valladares, C., and Su, S.: Longitudinal variability of equatorial plasma bubbles observed by DMSP and ROCSAT-1, Journal of Geophysical Research: Space Physics, 109, https://doi.org/10.1029/2004JA010583, 2004a.

Burke, W., Huang, C., Gentile, L., and Bauer, L.: Seasonal-longitudinal variability of equatorial plasma bubbles, Annales Geophysicae, 22, 3089–3098, https://doi.org/10.5194/angeo-22-3089-2004, 2004b.

Burke, W., de La Beaujardière, O., Gentile, L., Hunton, D., Pfaff, R., Roddy, P., Su, Y.-J., and Wilson, G.: C/NOFS observations of plasma density and electric field irregularities at post-midnight local times, Geophysical Research Letters, 36, L00C09, https://doi.org/10.1029/2009GL038879, 2009.

Carrano, C. S. and Groves, K. M.: TEC gradients and fluctuations at low latitudes measured with high data rate GPS receivers, in: Proceedings of the 63rd annual meeting of the Institute of Navigation, Cambridge, MA, pp. 156–163, 2007.

Carter, B. A., Zhang, K., Norman, R., Kumar, V. V., and Kumar, S.: On the occurrence of equatorial F-region irregularities during solar minimum using radio occultation measurements, Journal of Geophysical Research: Space Physics, 118, 892–904, https://doi.org/10.1002/jgra.50089, 2013.

Chu, C.-H., Fong, C.-J., Xia-Serafino, W., Shiau, A., Taylor, M., Chang, M.-S., Chen, W.-J., Liu, T.-Y., Liu, N.-C., Martins, B., Garcia, J. R., and Da Silva Curiel, A.: An Era of Constellation Observation-FORMOSAT-3/COSMIC and FORMOSAT-7/COSMIC-2, Journal of Aeronautics, Astronautics and Aviation, 50, 335–346, 2018.

Dao, E., Kelley, M., Roddy, P., Retterer, J., Ballenthin, J., de La Beaujardiere, O., and Su, Y.-J.: Longitudinal and seasonal dependence of nighttime equatorial plasma density irregularities during solar minimum detected on the C/NOFS satellite, Geophysical Research Letters, 38, https://doi.org/10.1029/2011GL047046, 2011.

Farley, D., Balsey, B., Woodman, R., and McClure, J.: Equatorial spread F: Implications of VHF radar observations, Journal of Geophysical Research, 75, 7199–7216, https://doi.org/10.1029/JA075i034p07199, 1970.

Fejer, B. G. and Kelley, M.: Ionospheric irregularities, Reviews of Geophysics, 18, 401–454, https://doi.org/10.1029/RG018i002p00401, 1980.

Fejer, B. G., Scherliess, L., and De Paula, E.: Effects of the vertical plasma drift velocity on the generation and evolution of equatorial spread F, Journal of Geophysical Research: Space Physics, 104, 19 859–19 869, https://doi.org/10.1029/1999JA900271, 1999.

Gentile, L., Burke, W., and Rich, F.: A global climatology for equatorial plasma bubbles in the topside ionosphere, 24, 163–172, https://hal.archives-ouvertes.fr/hal-00317925, 2006.

Hajj, G. A., Kursinski, E., Romans, L., Bertiger, W., and Leroy, S.: A technical description of atmospheric sounding by GPS occultation, Journal of Atmospheric and Solar-Terrestrial Physics, 64, 451–469, 2002.

Hanson, W. and Sanatani, S.: Large Ni gradients below the equatorial F peak, Journal of Geophysical Research, 78, 1167–1173, https://doi.org/10.1029/JA078i007p01167, 1973.

Huang, C., Burke, W., Machuzak, J., Gentile, L., and Sultan, P.: DMSP observations of equatorial plasma bubbles in the topside ionosphere near solar maximum, Journal of Geophysical Research: Space Physics, 106, 8131–8142, https://doi.org/10.1029/2000JA000319, 2001.

Huang, C.-S., de La Beaujardiere, O., Roddy, P., Hunton, D., Pfaff, R., Valladares, C., and Ballenthin, J.: Evolution of equatorial ionospheric plasma bubbles and formation of broad plasma depletions measured by the C/NOFS satellite during deep solar minimum, Journal of Geophysical Research: Space Physics, 116, https://doi.org/10.1029/2010JA015982, 2011.

Jakowski, N., Leitinger, R., and Angling, M.: Radio occultation techniques for probing the ionosphere, Annals of Geophysics, 47, 1049–1066, https://doi.org/10.4401/ag-3285, 2004.

Kelley, M.: The Earth's Ionosphere: Plasma Physics and Electrodynamics, International geophysics series, Academic Press, 2009.

Krall, J., Huba, J., Ossakow, S., and Joyce, G.: Why do equatorial ionospheric bubbles stop rising?, Geophysical Research Letters, 37, L09 105, https://doi.org/10.1029/2010GL043128, 2010.

Kudeki, E. and Bhattacharyya, S.: Postsunset vortex in equatorial F-region plasma drifts and implications for bottomside spread-F, Journal of Geophysical Research: Space Physics, 104, 28 163–28 170, https://doi.org/10.1029/1998JA900111, 1999.

Kudeki, E., Akgiray, A., Milla, M., Chau, J. L., and Hysell, D. L.: Equatorial spread-F initiation: Post-sunset vortex, thermospheric winds, gravity waves, Journal of Atmospheric and Solar-Terrestrial Physics, 69, 2416–2427, https://doi.org/10.1016/j.jastp.2007.04.012, 2007.

Kursinski, E. R., Hajj, G. A., Schofield, J. T., Linfield, R. P., and Hardy, K. R.: Observing Earth's atmosphere with radio occultation measurements using the Global Positioning System, Journal of Geophysical Research: Atmospheres, 102, 23 429–23 465, https://doi.org/10.1029/97JD01569, 1997.

Kursinski, E. R., Hajj, G. A., Leroy, S. S., and Herman, B.: The GPS Radio Occultation Technique, Terrestrial Atmospheric and Oceanic Sciences, 11, 53–114, http://hdl.handle.net/2014/14027, 1999.

Lei, J., Syndergaard, S., Burns, A. G., Solomon, S. C., Wang, W., Zeng, Z., Roble, R. G., Wu, Q., Kuo, Y.-H., Holt, J. M., et al.: Comparison of COSMIC ionospheric measurements with ground-based observations and model predictions: Preliminary results, Journal of Geophysical Research: Space Physics, 112, A07 308, https://doi.org/10.1029/2006JA012240, 2007.

Liu, J., Chen, S., Yeh, W., Tsai, H., and Rajesh, P.: Worst-case GPS scintillations on the ground estimated from radio occultation observations of FORMOSAT-3/COSMIC during 2007–2014, Surveys in Geophysics, 37, 791–809, https://doi.org/10.1007/s10712-015-9355-x, 2016.

Martinis, C. and Mendillo, M.: Equatorial spread F-related airglow depletions at Arecibo and conjugate observations, Journal of Geophysical Research: Space Physics, 112, A10 310, 2007.

McClure, J., Hanson, W., and Hoffman, J.: Plasma bubbles and irregularities in the equatorial ionosphere, Journal of Geophysical Research, 82, 2650–2656, https://doi.org/10.1029/JA082i019p02650, 1977.

McClure, J., Singh, S., Bamgboye, D., Johnson, F., and Kil, H.: Occurrence of equatorial F region irregularities: Evidence for tropospheric seeding, Journal of Geophysical Research: Space Physics, 103, 29 119–29 135, https://doi.org/10.1029/98JA02749, 1998.

Nishioka, M., Saito, A., and Tsugawa, T.: Occurrence characteristics of plasma bubble derived from global ground-based GPS receiver networks, Journal of Geophysical Research: Space Physics, 113, A05 301, https://doi.org/10.1029/2007JA012605, 2008.

Park, J., Min, K. W., Kim, V. P., Kil, H., Lee, J.-J., Kim, H.-J., Lee, E., and Lee, D. Y.: Global distribution of equatorial plasma bubbles in the premidnight sector during solar maximum as observed by KOMPSAT-1 and Defense Meteorological Satellite Program F15, Journal of Geophysical Research: Space Physics, 110, A07 308, https://doi.org/10.1029/2004JA010817, 2005.

Retterer, J. and Roddy, P.: Faith in a seed: on the origins of equatorial plasma bubbles, Annales Geophysicae, 32, 485–498, https://doi.org/:10.5194/angeo-32-485-2014, 2014.

Rocken, C., Anthes, R., Exner, M., Hunt, D., Sokolovskiy, S., Ware, R., Gorbunov, M., Schreiner, W., Feng, D., Herman, B., Kuo, Y.-H., and Zou, X.: Analysis and validation of GPS/MET data in the neutral atmosphere, Journal of Geophysical Research: Atmospheres, 102, 29 849–29 866, https://doi.org/10.1029/97JD02400, 1997.

Röttger, J.: Equatorial spread-F by electric fields and atmospheric gravity waves generated by thunderstorms, Journal of Atmospheric and Terrestrial Physics, 43, 453–462, https://doi.org/10.1016/0021-9169(81)90108-2, 1981.

Sahai, Y., Aarons, J., Mendillo, M., Baumgardner, J., Bittencourt, J., and Takahashi, H.: OI 630 nm imaging observations of equatorial plasma depletions at 16 S dip latitude, Journal of Atmospheric and Terrestrial Physics, 56, 1461–1475, https://doi.org/10.1016/0021-9169(94)90113-9, 1994.

Sahai, Y., Fagundes, P., and Bittencourt, J.: Transequatorial F-region ionospheric plasma bubbles: solar cycle effects, Journal of Atmospheric and Solar-Terrestrial Physics, 62, 1377–1383, https://doi.org/10.1016/S1364-6826(00)00179-6, 2000.

Singh, S., Johnson, F., and Power, R.: Gravity wave seeding of equatorial plasma bubbles, Journal of Geophysical Research: Space Physics, 102, 7399–7410, https://doi.org/10.1029/96JA03998, 1997.

Stolle, C., Lühr, H., Rother, M., and Balasis, G.: Magnetic signatures of equatorial spread F as observed by the CHAMP satellite, Journal of Geophysical Research: Space Physics, 111, A02 304, https://doi.org/10.1029/2005JA011184, 2006.

Stolle, C., Lühr, H., and Fejer, B.: Relation between the occurrence rate of ESF and the equatorial vertical plasma drift velocity at sunset derived from global observations, Annales Geophysicae, 26, 3979–3988, https://doi.org/10.5194/angeo-26-3979-2008, 2008.

Su, S.-Y., Chao, C., and Liu, C.: On monthly/seasonal/longitudinal variations of equatorial irregularity occurrences and their relationship with the postsunset vertical drift velocities, Journal of Geophysical Research: Space Physics, 113, A05 307, https://doi.org/10.1029/2007JA012809, 2008.

Su, S.-Y., Wu, C. L., and Liu, C. H.: Correlation between the global occurrences of ionospheric irregularities and deep atmospheric convective clouds in the intertropical convergence zone (ITCZ), Earth, Planets and Space, 66, 134 1 – 134 8, https://doi.org/10.1186/1880-5981-66-134, 2014.

Sultan, P.: Linear theory and modeling of the Rayleigh-Taylor instability leading to the occurrence of equatorial spread F, Journal of Geophysical Research: Space Physics, 101, 26 875–26 891, https://doi.org/10.1029/96JA00682, 1996.

Syndergaard, S.: COSMIC S4 Data, COSMIC Data Analysis and Archival Center at UCAR, https://tacc.cwb.gov.tw/cdaac/doc/documents/s4_description.pdf, 2006.

Taori, A., Patra, A., and Joshi, L.: Gravity wave seeding of equatorial plasma bubbles: An investigation with simultaneous F region, E region, and middle atmospheric measurements, Journal of Geophysical Research: Space Physics, 116, A05 310, https://doi.org/10.1029/2010JA016229, 2011.

Tsai, L.-C., Su, S.-Y., and Liu, C.-H.: Global morphology of ionospheric F-layer scintillations using FS3/COSMIC GPS radio occultation data, GPS Solutions, 21, 1037–1048, https://doi.org/10.1007/s10291-016-0591-4, 2017.

Tsunoda, R. T.: Magnetic-field-aligned characteristics of plasma bubbles in the nighttime equatorial ionosphere, Journal of Atmospheric and Terrestrial Physics, 42, 743–752, https://doi.org/10.1016/0021-9169(80)90057-4, 1980.

Tsunoda, R. T.: Control of the seasonal and longitudinal occurrence of equatorial scintillations by the longitudinal gradient in integrated E region Pedersen conductivity, Journal of Geophysical Research: Space Physics, 90, 447–456, https://doi.org/10.1029/JA090iA01p00447, 1985.

Tsunoda, R. T.: Seeding of equatorial plasma bubbles with electric fields from an Es-layer instability, Journal of Geophysical Research: Space Physics, 112, A06 304, https://doi.org/10.1029/2006JA012103, 2007.

Tsunoda, R. T.: On seeding equatorial spread F: Circular gravity waves, Geophysical Research Letters, 37, L10 104, https://doi.org/10.1029/2010GL043422, 2010.

Tsunoda, R. T.: Upwelling: a unit of disturbance in equatorial spread F, Progress in Earth and Planetary Science, 2, 9, https://doi.org/10.1186/s40645-015-0038-5, 2015.

Whalen, J.: Equatorial bubbles observed at the north and south anomaly crests: Dependence on season, local time, and dip latitude, Radio Science, 32, 1559–1566, https://doi.org/10.1029/97RS00285, 1997.

Wickert, J., Reigber, C., Beyerle, G., König, R., Marquardt, C., Schmidt, T., Grunwaldt, L., Galas, R., Meehan, T. K., Melbourne, W. G., and Hocke, K.: Atmosphere sounding by GPS radio occultation: First results from CHAMP, Geophysical Research Letters, 28, 3263–3266, https://doi.org/10.1029/2001GL013117, 2001.

Wickert, J., Beyerle, G., Hajj, G. A., Schwieger, V., and Reigber, C.: GPS radio occultation with CHAMP: Atmospheric profiling utilizing the space-based single difference technique, Geophysical Research Letters, 29, 1–4, https://doi.org/10.1029/2001GL013982, 2002.

Wickert, J., Schmidt, T., Beyerle, G., König, R., Reigber, C., and Jakowski, N.: The radio occultation experiment aboard CHAMP: Operational data analysis and validation of vertical atmospheric profiles, Journal of the Meteorological Society of Japan. Ser. II, 82, 381–395, https://doi.org/10.2151/jmsj.2004.381, 2004.

Wickert, J., Michalak, G., Schmidt, T., Beyerle, G., Cheng, C.-Z., Healy, S. B., Heise, S., Huang, C.-Y., Jakowski, N., Köhler, W., Mayer, C., Offiler, D., Ozawa, E., Pavelyev, A., Rothacher, M., Tapley, B., and Arras, C.: GPS Radio Occultation: results from CHAMP, GRACE and FORMOSAT-3/COSMIC., Terrestrial, Atmospheric & Oceanic Sciences, 20, 35–50, https://doi.org/: 10.3319/TAO.2007.12.26.01(F3C), 2009.

Woodman, R. F.: Spread F – an old equatorial aeronomy problem finally resolved?, Annales Geophysicae, 27, 1915–1934, https://doi.org/10.5194/angeo-27-1915-2009, 2009.

Woodman, R. F. and La Hoz, C.: Radar observations of F region equatorial irregularities, Journal of Geophysical Research, 81, 5447–5466, https://doi.org/10.1029/JA081i031p05447, 1976.

Xiong, C., Park, J., Lühr, H., Stolle, C., and Ma, S.: Comparing plasma bubble occurrence rates at CHAMP and GRACE altitudes during high and low solar activity, Annales Geophysicae, 28, 1647, 2010.

Yeh, K. C. and Liu, C.-H.: Radio wave scintillations in the ionosphere, Proceedings of the IEEE, 70, 324–360, https://doi.org/10.1109/PROC.1982.12313, 1982.

Yokoyama, T.: A review on the numerical simulation of equatorial plasma bubbles toward scintillation evaluation and forecasting, Progress in Earth and Planetary Science, 4, 37, https://doi.org/10.1186/s40645-017-0153-6, 2017.